DEVELOPMENT OF A NONINVASIVE CALCIUM IMAGING PROBE

by

Joel Robert Pieper

A thesis submitted to the faculty of
The University of Utah
in partial fulfillment of the requirements for the degree of

Master of Science

Department of Bioengineering

The University of Utah

August 2013

The University of Utah Graduate School

STATEMENT OF THESIS APPROVAL

The thesis of **Joel Robert Pieper**

has been approved by the following supervisory committee members:

Edward Hsu	, Chair	**6/14/2013** Date Approved
John Phillips	, Member	**6/14/2013** Date Approved
Frank Sachse	, Member	Date Approved

and by **Patrick A. Tresco** , Chair of the Department of **Bioengineering**

and by Donna M. White, Interim Dean of The Graduate School.

ABSTRACT

Genetically encoded calcium indicators (GECIs) are Ca^{2+} sensitive fluorescent proteins that have expanded the usefulness of optical calcium imaging to longitudinal *in vivo* studies due to their advantage of direct expression in the tissue being imaged. Several generations of GECIs have been developed using green fluorescent protein (GFP) or one of its variants with each generation improving upon Ca^{2+}-binding affinities and optical properties. However, the tissue penetration of excitation or emission light through tissue is small due to high absorption of available GECI wavelengths, which are shorter than the infrared range. The field still lacks a GECI with excitation or emission wavelengths in the infrared range, which has significantly less attenuation in biological tissue. Here we propose the development of an infrared GECI by insertion of the Ca^{2+}-binding domain calmodulin (CaM) into regions surrounding the biliverdin chromophore binding pocket of infrared fluorescent protein (iRFP). We proposed seven DNA constructs of iRFP with different CaM insertion sites. Six of the seven DNA constructs were successfully produced with protein expressed from one of these constructs exhibiting similar optical properties to iRFP, showing successful receptor insertion into iRFP. Though our initial Ca^{2+} sensitivity test to monitor change in fluorescence due to Ca^{2+} binding is not conclusive, we open the field of GECI engineering to exciting new possibilities for noninvasive deep tissue calcium imaging.

TABLE OF CONTENTS

ABSTRACT.....iii

LIST OF FIGURES….....v

INTRODUCTION.....1

Biological Role of Calcium.....1
Calcium Imaging.....3
Calcium Dyes.....4
Genetically Encoded Calcium Indicators.....6
GECI Calcium Binding Affinities.....8
Advantages of Infrared Imaging.....9
Experimental Aims.....10

MATERIALS AND METHODS.....12

Construct Design.....12
Construct Fragment Production.....15
Fragment Ligation Procedure.....18
Protein Purification and Optical Characterization.....19

RESULTS.....22

DISCUSSION.....29

REFERENCES.....32

LIST OF FIGURES

Figure Page

1. Calmodulin ligation sites in iRFP for construct development.....13

2. Primary structures of final constructs.....14

3. Primer setup for PCR method of acquiring fragments A, B and C.....15

4. Ligation method for creating final constructs.....18

5. Digestion confirming proper fragment construction.....23

6. Expression results for WT iRFP and constructs.....24

7. Pelleted cultures showing green hue for WT iRFP and C1.....25

8. Absorbance spectra for iRFP and free biliverdin.....26

9. Ni-NTA batch purification of C1.....26

10. Absorbance spectra for WT iRFP and C1.....27

11. Emission spectra for C1 in the absence and presence of calcium ions.....28

INTRODUCTION

Biological Role of Calcium

The calcium ion (Ca^{2+}) performs diverse functions in cell signaling and physiology, including cellular differentiation, motility, proliferation, apoptosis, gene transcription and more specialized roles in excitable cells [1]. Increase in intracellular Ca^{2+} concentration ($[Ca^{2+}]_i$) is responsible for release of neurotransmitter vesicles from presynaptic neurons and synaptic plasticity in postsynaptic neurons. In muscle cells, transient increases in $[Ca^{2+}]_i$ underlie the coupling between electrical excitation and mechanical contraction [2].

Ca^{2+} induced Ca^{2+} release is the means by which calcium transients mediate excitation-contraction coupling in cardiomyocytes. Upon depolarization of the cardiomyocyte, L-type Ca^{2+} channels localized in the cell membrane along transverse tubules pass calcium ions down their electrochemical gradient into the cell. These Ca^{2+} ions interact with ryanodine receptors (RyR) in the membrane of the sarcoplasmic reticulum (SR) which is located near the T-tubules. Upon binding of Ca^{2+}, RyRs release large amounts of calcium ions from the SR into the cytosol, increasing $[Ca^{2+}]_i$ 10-fold from around 100 nM to more than 1 μM [2].

Calcium ions diffuse to the actin and myosin contractile fibers where they become chelated in site II of the regulatory domain of troponin C (TnC). This event alters the structure of the regulatory domain, exposing hydrophobic residues that interact with

troponin I (TnI), disrupting its inhibitory effect on actin-myosin interactions [3]. Once allowed to interact, myosin heads walk along actin filaments, consuming ATP and shortening sarcomere length which produces contraction in the activated cardiomyocyte. Myocyte contraction is a transitory event because free Ca^{2+} ions in the cytosol are continually sequestered back into the SR through the sarco/endoplasmic reticulum ATPase (SERCA) and removed from the cell through Ca^{2+} pumps and the Na^{+}-Ca^{2+} exchanger (NCX).

Alterations of calcium handling in the excitation-contraction process are known to occur in cardiac disease [2]. For instance, total Ca^{2+} content of cardiomyocytes is known to be decreased in some types of heart failure. With less available Ca^{2+} to interact with contractile elements, the total force of contraction is lessened, decreasing the heart's pumping efficiency. Overloading of Ca^{2+} in the SR along with increased sensitivity in RyR can cause spontaneous Ca^{2+} leaks into the cytosol [2]. This spontaneous increase in $[Ca^{2+}]_i$ during diastole is countered by increased activity in NCX. Because three Na^{+} ions are brought into the cell for each Ca^{2+} ion exiting, there is a net inward current that causes early (EAD) or delayed (DAD) afterdepolarization. This depolarization can lead to extrasystoles that may be arrhythmogenic.

Monitoring changes in calcium handling during disease development and treatment in cells and tissue preparations has been of great importance for understanding cellular mechanisms. In monitoring the spatial distribution of Ca^{2+} ions within whole tissues and subcellular compartments, optical calcium imaging has been an indispensable technique. This imaging technique makes use of a diverse range of calcium probes (Ca^{2+}-chelating structures coupled with fluorescent moieties) in order to report changes in Ca^{2+} concentration as changes in fluorescence intensity.

Calcium Imaging

Fluorescence is the process by which a molecule absorbs and emits photon energy. It occurs after photon energy is absorbed by and thereby excites a ground state electron in the molecule, moving it into a higher energy state [4]. After dissipation of some vibrational energy, the electron will return to the ground state, emitting the remaining absorbed energy in the form of a photon with less energy and longer wavelength than the absorbed photon. The fluorescence phenomenon occurs seemingly instantaneously following excitation. The difference between excitation and emission wavelengths of a fluorescent molecule is known as the Stoke's shift. Imaging fluorescent molecules at their emission wavelength during excitation allows localization of the fluorescent molecule. When a fluorescent molecule preferentially localizes to a particular region or colocalizes with another molecule, it is considered a probe, because it allows spatial visualization of a particular space or target molecule. Calcium probes display quenching or alteration of fluorescence when Ca^{2+} is not bound which decreases background signal where there is no Ca^{2+} for the probe to bind.

Two classes of fluorescent calcium probes currently exist [5]. The first class consists of calcium dyes, which are small synthetic molecules that change fluorescence upon chelating Ca^{2+} ion. The second class is genetically encoded calcium indicators (GECIs), which are fluorescent proteins that are Ca^{2+} sensitive due to fusion of a fluorescent protein with a Ca^{2+}-binding peptide. There are strengths and limitations associated with both of these classes of probes that should be taken into account before use in calcium imaging procedures.

Calcium Dyes

Commonly used calcium dyes include fura-2, rhod-2 and fluo-4. These dyes utilize stilbene, rhodamine and fluorescein as their respective fluorescent moieties, each of which is coupled with the BAPTA Ca^{2+} chelating moiety. The BAPTA moiety contains high electron density which is able to be donated into the highly conjugated fluorescent moieties. When Ca^{2+} becomes chelated by the oxygen atoms in BAPTA, electron density donation is decreased, increasing fluorescence intensity or shifting excitation or emission wavelength peaks of the molecule [6]. Because of the large negative charge on the BAPTA moiety, the carboxylate ions are derivitized as acetoxymethyl esters (AM) to give the molecule a neutral charge, allowing it to diffuse across cell membranes. These AM derivatives are then cleaved with endogenous intracellular esterases, restoring the negative charge and preventing the calcium dye from diffusing back out of the cell.

The on/off kinetics for the BAPTA-derived calcium dyes is typically around 2/100 ms, a highly desirable property when used to visualize short-lived calcium transients [5]. They also have calcium affinities that are beneficial for monitoring physiologic changes in $[Ca^{2+}]_i$. These binding affinities are generally reported as dissociation constants (K_d), which is the concentration of Ca^{2+} at which half of the species in solution are bound to Ca^{2+}. Calcium dyes generally have K_ds ranging from 200 to 600 nM, with some desirable exceptions.

Fura-2 is one of the oldest available calcium dyes and is still used frequently due to its ratiometric property [7]. Binding of Ca^{2+} (K_d = 224 nM) shifts the excitation wavelength from 380 to 340 nm while keeping emission at 510 nm. This allows a more

quantitative measure of $[Ca^{2+}]_i$ as the ratiometric fluorescence imaging method is not dependent upon the concentration of calcium dye in the cell.

The use of fluo-4 quickly caught on due to its wavelength compatibility (494/516 nm ex/em) with fluorescein optical filter sets already available at the time [8] and its 120-fold increase in fluorescence intensity upon binding Ca^{2+} (K_d = 350 nM). Rhod-2 is also an intensiometric calcium dye with 552/581 ex/em fluorescence wavelengths and a K_d of 570 nM. These optical properties are more red-shifted than fura-2 or fluo-4. Another benefit to rhod-2 is that it is preferentially taken up into the mitochondrial subcellular compartment because it contains a net positive charge as an AM derivative [9]. However, its use as a mitochondrial Ca^{2+} reporter is much improved when reduced to dihydro-rhod-2-AM, which experiences fluorescence quenching until oxidized in the mitochondria to rhod-2. This helps to prevent simultaneous reporting of cytosolic $[Ca^{2+}]$.

Other methods have been used to increase the ability to localize calcium dyes or alter their Ca^{2+} affinities for more specified applications. Boca-1 BG (522/536 ex/em and 200 nM K_d) has a 180-fold change in fluorescence intensity and has been developed to covalently bind to SNAP-tagged proteins, making it able to colocalize into desired subcellular spaces [10]. X-Rhod-5F has been engineered with decreased Ca^{2+} binding affinity (1.6 μM K_d), making it more useful for imaging in regions with high basal $[Ca^{2+}]$ such as the endoplasmic reticulum.

KFCA is a more recently developed calcium dye that has excitation and emission wavelengths in the near infrared range [11]. This contains a BODIPY based fluorescent moiety with sharp 650/660 nm ex/em peaks and a K_d of 500 nM. Similar to fluo-4, KFCA also experiences 120-fold change in fluorescence intensity upon binding Ca^{2+}. The far red shifted wavelengths of this calcium dye are of particular interest to deep tissue imaging.

While calcium dyes are more easily applied in experimental application and can be more easily engineered to obtain desired Ca^{2+}-binding affinities and fluorescence change, they suffer major limitations for longitudinal (repeatable studies over the lifetime of a subject) and noninvasive use *in vivo*. Because calcium dyes are delivered to the cytosol via passive diffusion across the cell membrane, the dye loading process requires removal of tissue for bathing in a dye-containing solution or invasive perfusion procedures if done without tissue removal [12]. This process is also nonselective with regard to cell type and undesirable background signal lowers signal to noise ratio during imaging. Cell-specific delivery of calcium dyes can also be done by patch pipette, but this technique is impractical for multicellular tissue imaging. Dyes also suffer from wash out from the cell, decreasing signal intensity over the course of imaging. These limitations prohibit noninvasive application of calcium dyes for *in vivo* calcium imaging.

Genetically Encoded Calcium Indicators

GECIs have been largely complementary to calcium dyes' abilities. Though GECIs suffer from smaller changes in fluorescence and more limited Ca^{2+}-binding affinities, they have the advantage of being expressed *in vivo*. The gene encoding a GECI can be delivered to the nucleus of a cell via transfection [13], viral transduction [14] or development of a transgenic organism [15]. Localization of expression can also be highly specific when coupled with tissue-specific promoters and/or subcellular localization tags [16, 17]. These strengths make GECIs an efficient tool for noninvasive calcium imaging *in vivo*.

GECI engineering has previously been achieved by either fusion of a single fluorescent protein (variants of green fluorescent protein (GFP)) with a Ca^{2+}-binding

peptide [18] or connecting two fluorescent proteins with a Ca^{2+}-binding peptide and a peptide that can interact with the Ca^{2+}-binding peptide [19, 20, 21]. The former method produces changes in fluorescence intensity while the latter can make use of Förster resonance energy transfer (FRET) to provide a change in the ratio of intensities of two emission wavelengths. Examples from each of these types of GECIs include camgaroo [18], GCaMP [19] and cameleon [20].

Camgaroo was produced by replacing the 145^{th} amino acid of a GFP-like protein with the Ca^{2+}-binding peptide calmodulin (CaM) [18]. Ca^{2+} and pH titrations revealed that the binding of Ca^{2+} to the fused CaM domain alters its structure in a similar manner to TnC (a close relative of CaM) which causes deprotonation of the chromophore, changing the ratio of 400 nm to 490 nm emission. GCaMP also utilizes fusion of CaM to GFP, however, the GFP is circularly permuted (cp) and CaM is placed at the end of cpGFP while the CaM-binding peptide of myosin light chain kinase (M13) is placed at the beginning of cpGFP [19]. The fluorescence intensity change in GCaMP is due to M13 interacting with CaM after CaM binds Ca^{2+}, thereby restoring natural GFP chromophore structure by bringing the two ends of cpGFP closer together [22].

The FRET-based cameleon is produced by using CaM and M13 to link two different GFP-like proteins (such as YFP and CFP) together [20]. Upon binding of Ca^{2+} to CaM, M13 folds in to interact with CaM, bringing YFP closer to CFP. When CFP is excited at 440 nm, it undergoes nonradiative FRET with YFP causing the YFP chromophore to emit 535 nm wavelength light. In the absence of Ca^{2+}, fluorescence emission from only the CFP is detected at 480 nm. Variants on cameleon have also been produced using TnC instead of CaM as the Ca^{2+}-binding domain and TnI instead of M13

as the interaction peptide in an effort to prevent interaction of the fused CaM domain with targets of its multiple cellular signaling pathways [21].

GECI Calcium Binding Affinities

CaM and TnC are effective fusion inserts for conferring Ca^{2+} sensitivity to fluorescent proteins due to their Ca^{2+}-chelating structure. Both belong to a dumb-bell shaped protein family containing two domains (N and C) linked by a flexible strand of amino acids. Each domain contains two Ca^{2+}-chelating sites (I and II on the N domain and III and IV on the C domain) in the form of EF hand motifs that are two helices (E and F) connected by a loop containing multiple negatively charged residues involved in Ca^{2+} chelation. The helices comprising the EF hands change conformation with respect to one another when Ca^{2+} binds to the loop between them, exposing previously buried hydrophobic residues. These activated regions can then bind to a number of different targets within the cell including TnI and actin for the N and C domains of TnC, respectively [3], and a host of different targets for CaM [23]. When ligated into particular regions around the chromophore of fluorescent proteins, these domains will bind Ca^{2+} ions and change conformation, affecting the fluorescence intensity of the fluorescent protein with which they are fused.

The Ca^{2+}-binding affinities of the CaM and TnC inserts are important to consider when designing a GECI. The N and C terminal domains of CaM and TnC consist of Ca^{2+}-binding sites I/II and III/IV, respectively. CaM N and C terminal K_d have been measured at 2.4 μM and 18 μM [24]. The N terminal domain of skeletal troponin C (sTnC) has a much lower affinity for Ca^{2+} (K_d = 32 μM) compared to the C terminal domain (K_d = 200 nM) [25, 26]. Cardiac troponin C (cTnC) differs from sTnC in that site

I is nonfunctional and site II has about 10-fold more affinity (K_d = 3.8 μM) compared to the N terminal of sTnC [27]. Presence of M13 with CaM increases its Ca^{2+} affinity nearly 100-fold to a K_d of 26 nM [24]; and interestingly, when M13 is fused to the C terminal of CaM with a GG linker, there is a biphasic response with K_ds of 80 nM and 2 μM with an overall K_d of around 500 nM.

These Ca^{2+} affinities affect the GECIs in which they are incorporated but a GECI's K_d is not necessarily the same as the insert it contains. For instance, camgaroo, which contains the CaM insert, has a K_d of 7 μM which is similar to the overall biphasic response of CaM N and C terminal Ca^{2+} binding [18]. But, the CaM and M13 containing GECI GCaMP has a K_d of 235 nM compared to the 26 nM K_d of the CaM and M13 peptides alone [19]. The cameleon derivatives with CaM and M13 fusion may have similar or much lower affinities compared to the CaMM13 hybrid molecule [14]. The receptor insert used in our study was CaM.

Advantages of Infrared Imaging

With all of the successful GECIs heretofore engineered, GECIs' full potential as noninvasive *in vivo* calcium probes has not yet been realized. This is because GECIs are not yet available in the infrared range (700 to 1,000 nm) for excitation or emission wavelengths. The infrared wavelength range exhibits both decreased attenuation and detectable autofluorescence in biological tissue [28]. Thus, although GECIs are expressed *in vivo*, imaging still requires removal or exposure of the tissue being imaged for either penetration of excitation wavelength light to the tissue or visualization of the emission wavelength signal produced in the tissue.

Another incentive to move imaging into the infrared range is the recent development of an exciting new optical imaging technique known as fluorescence molecular tomography (FMT) that is able to calculate a pseudo 3D distribution of fluorophores in biological tissue [29]. A point source of light is applied below the scan subject at many locations and an image of the light transmitted through the subject is acquired from above for each location of the point source applied below. This process is performed with the point source set to the emission wavelength of the fluorophore, where there is no fluorescence detected, and the camera filtered to only receive light at the emission wavelength. This allows mapping of the diffusion and attenuation of light through the tissue being imaged. The same scan is then performed with the point source set to the excitation wavelength of the fluorophore and the camera still detecting emission wavelength light. In this manner, the only signal detected by the camera is originating from the locations of the fluorophores. These scan data are fed into complex algorithms describing the propagation of light through tissue, creating an inverse problem that can be solved by regularization and a number of techniques including singular value decomposition. The solution is a quantitative distribution of fluorophore intensity in the tissue.

Experimental Aims

The purpose of the current study is to propose that an infrared fluorescent protein could be used with the previously outlined GECI engineering techniques to produce a Ca^{2+} sensitive infrared fluorescent protein (an infrared GECI). This novel calcium probe will enable calcium imaging of deeper tissues, allowing noninvasive calcium imaging *in*

vivo. We seek to accomplish development of this novel tool by inserting CaM into a recently developed infrared fluorescent protein known as iRFP.

The infrared fluorescent protein we chose for testing was one recently developed by Filonov et. al. and termed iRFP [30]. iRFP is derived from a Rhodopseudomonas palustris bacteriophytochrome (RpBphP2) and has more than twice the signal to background ratio *in vivo* compared to far red GFP variants and around 18-fold higher brightness compared to the previously used infrared protein IFP1.4. iRFP covalently binds the tetrapyrrole biliverdin to form its chromophore, giving the protein a green color due to the high absorbance in the 350 to 450 nm wavelength range by biliverdin's conjugated pi system and producing fluorescence emission at 715 nm when excited with 690 nm light. We propose that introducing Ca^{2+} sensitivity into iRFP's infrared excitation and emission wavelengths would produce an infrared GECI that would allow *in vivo* calcium imaging at depths not currently attainable. When such a tool is used with FMT, pseudo 3D calcium imaging may be achievable where only 2D surface mapping has typically been reported with currently available GECIs.

MATERIALS AND METHODS

Construct Design

The primary structures of RpBphP3 (a close relative of RpBphP2), RpBphP2, iRFP, and CaM in addition to the available crystalline structure of RpBphP3 [31] and CaM [32] were viewed in PyMOL as templates for construct design. We first identified residues in the RpBphP3 crystalline structure that were involved with biliverdin chromophore binding [31]. Then we identified pi conjugated His, Phe, Tyr, and Trp residues facing toward the chromophore that might be involved in establishing the fluorescence properties of iRFP. Sites in the immediate vicinity of the chromophore were then identified that, after removal of a number of amino acid residues, could spatially accommodate insertion of the CaM protein crystalline structure (residues A2-A148) as determined by loading both structures into the same PyMOL session and placing them in a conformation that may be adopted in the final GECI structure.

We wanted the protein domains of the designed constructs to fold in such a way that they adopted similar structures to those resolved separately for iRFP and CaM. If they folded in this manner, the biliverdin chromophore binding pocket could be maintained in the new protein constructs while allowing slight changes in CaM conformation due to Ca^{2+} binding to cause minor changes in the locations of the identified pi conjugated residues with respect to the chromophore. Seven ligation sites were chosen that met these criteria (Figure 1) where we would replace one or more

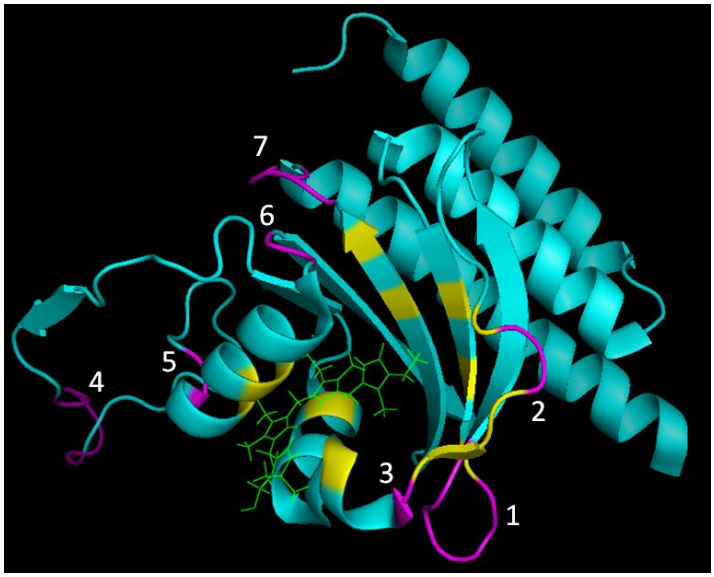

Figure 1 – Calmodulin ligation sites in iRFP for construct development. Crystalline structure of RpBphP3, a close relative to iRFP, shown with biliverdin chromophore (green) [31]. Seven ligation sites are in magenta, numbered from 1 to 7. These residues were replaced by CaM with the GAP and VD linker peptides. Residues colored in yellow are known to interact with chromophore binding or have conjugated pi systems.

residues of iRFP with the CaM insert and linker peptides (GAP linker on N terminal of CaM and VD linker on C terminal of CaM). With insertion of CaM in these regions, Ca^{2+}-induced conformational changes of the CaM insert might affect a change in iRFP chromophore structure thereby making its fluorescence properties Ca^{2+} sensitive.

Considerable flexibility was assumed in the linker peptides and strand connecting the N and C domains of CaM such that the distance between the N and C terminals of the CaM insert could span the length of residues removed at each site. As such, residues 211-216 were removed for ligation at site 1. Likewise, residues 231-232, 236, 270-276, 288-289, 301-302, and 324-329 were removed for ligation into sites 2, 3, 4, 5, 6 and 7. We recognize the highly speculative nature of this method of construct design. More robust methods may have been used such as molecular modeling. However, there is no resolved

structure available for iRFP which would be ideal for molecular modeling. Also, due to the many advances in molecular cloning techniques, computational studies would take considerably more time to perform than generating a number of different constructs through molecular biology cloning techniques.

Thus, seven DNA constructs (designated C1-C7) were designed which were sequentially composed of the portion of the iRFP gene upstream of a ligation site, the CaM gene insert and the portion of the iRFP gene downstream of a ligation site (Figure 2). For each of the seven constructs, the portion of the iRFP gene upstream of the ligation site was termed fragment A and the downstream portion was termed fragment C. These unique fragments were also numbered according to the construct they would comprise.

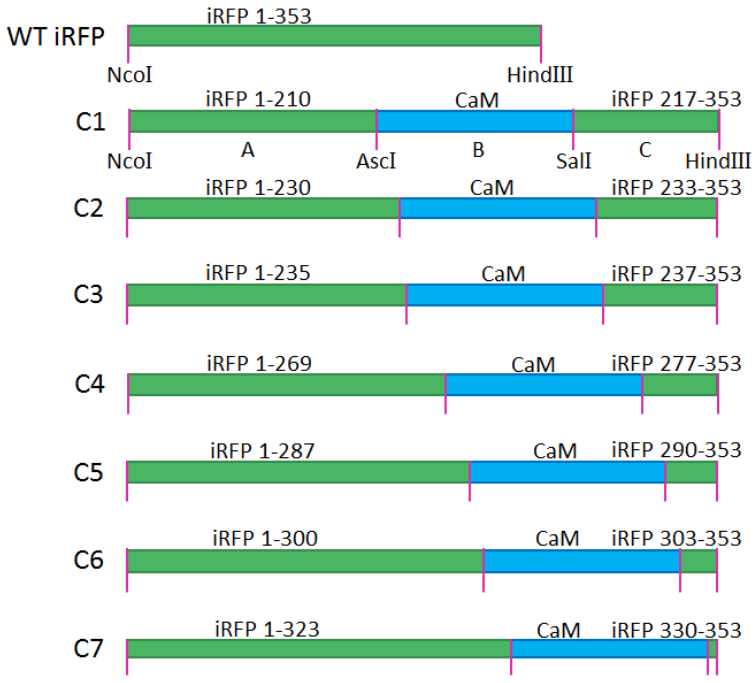

Figure 2 – Primary structures of final constructs. Constructs consist of fragments A, B and C joined by restriction sites AscI and SalI and framed by NcoI and HindIII restriction sites. Green fragments (A and B) are the indicated residues of wild type iRFP (WT iRFP) while the blue fragment (B) is residues 2-148 of calmodulin (CaM).

The common CaM insert was termed fragment B for each construct. Altogether, fragments A, B (450 bp) and C make open reading frames (ORF) which translate to proteins around 500 amino acid (AA) residues for the novel constructs. The final protein constructs are around 55 kDa in size.

Construct Fragment Production

The pBAD/His-B-iRFP and pDONR223-CALM3 plasmids deposited by Vladislav Verkhusha [30] and William Hahn [33], respectively, were obtained from Addgene. Polymerase chain reaction (PCR) was used to amplify the A, B and C fragments that would compose the DNA constructs similar to the method performed for the production of camgaroo (Figure 3) [18]. The common B fragment was amplified using oligonucleotide primers designed to have 3' ends complementary to the ends of the CALM3 insert in the pDONR223-CALM3 plasmid with 5' ends containing the nucleotides coding for an AscI restriction site on the sense primer and a SalI restriction

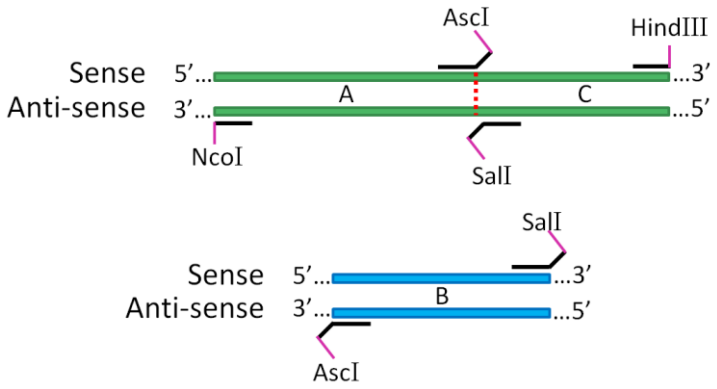

Figure 3 – Primer setup for PCR method of acquiring fragments A, B and C. Green double stranded DNA is iRFP. Blue double stranded DNA is CaM. Ligation site is shown as red dashed line. Restriction site sequences for AscI and SalI were contained within the portion of the primer that was not complementary to the original DNA sequence.

site on the antisense primer. For fragment A amplification, a common sense primer matching the 5’ end of the iRFP sense strand was used with one of seven unique antisense primers with 3’ ends designed to match the iRFP antisense strand just upstream of their respective ligation sites and 5’ ends that contain nucleotides coding the AscI restriction site. Likewise, for fragment C amplification, a common antisense primer matching the 5’ end of the iRFP antisense strand was used with one of seven unique sense primers with 3’ ends designed to match the iRFP sense strand just downstream of their respective ligation sites and 5’ ends that contain nucleotides coding the SalI restriction site. The iRFP gene already contained an N terminal His tag and was flanked by restriction sites NcoI and HindIII which were incorporated into the common sense and antisense primers. Because PCR primer cooperation is essential to fragment amplification, all primer pairs needed to have similar melting temperatures (Tm). The amount of GC content in unique primers for sites 3, 4, 5 and 7 required use with longer versions of the common sense or antisense primers. Variations of antisense primers for 5A and 7A were also produced due to difficult PCR reactions. These primers contained complementary regions before and after the AscI-coding nucleotides. All primers ensured that the final constructs would be in frame after ligations were completed.

PCR was performed with Platinum Taq DNA Polymerase from Invitrogen according to the recommended protocol with 2 mM $MgCl_2$. Fresh PCR product was ran on a 0.7% agarose gel stained with ethidium bromide (EtBr) to confirm presence of fragment with the desired length and visualize fragments of incorrect lengths that resulted from nonspecific primer binding. For reactions that resulted in no visible bands on agarose gel, the concentration of $MgCl_2$ was increased to 3 mM to promote primer binding at the expense of nonspecific binding.

The fresh PCR product fragments generated by Taq polymerase contained single 3’ adenine overhangs on each strand when amplified in the absence of a proofreading polymerase. These fragments could then be TOPO-cloned using a TOPO TA cloning kit from Invitrogen into linear pCR2.1-TOPO vector, which contains 3’ thymine overhangs in the cloning ORF, using topoisomerase enzyme. TOPO cloning creates a PCR fragment-containing circular plasmid that can be replicated when transformed into DH5α bacterial cells and plated on LB plates containing 50 μg/mL kanamycin and 40 μL of both 40 mg/mL X-Gal and 100 mM IPTG. Because the fragment cloning site in pCR2.1-TOPO is contained in a LacZα ORF which codes for the beta-galactosidase enzyme, insertion of a fragment disrupts production of this enzyme which normally converts X-Gal into blue products when expressed with IPTG. Therefore, bacterial colonies containing fragment insertions are white compared to the blue colonies containing pCR2.1-TOPO vector with no PCR fragment insertion.

White colonies were selected and grown in 10 mL LB overnight cultures to amplify fragment-containing plasmids. Plasmids were isolated with a QIAGEN Plasmid Mini kit and digested in New England Biolabs (NEB) recommended restriction enzyme buffers with restriction enzymes corresponding to the fragment’s unique restriction site and another compatible site in the pCR2.1-TOPO vector (NcoI and AscI for fragment A, NcoI and SalI for fragment B, EcoRI and HindIII for fragment C) and run on 0.7% agarose gels to ensure correct fragment sizes and determine fragment orientation in the cloning site. For plasmids containing the correct fragment size, M13 forward and reverse primers were added in separate samples and sent to the DNA sequencing core to ensure no deleterious mutations resulted from PCR amplification of the fragments.

Fragment Ligation Procedure

When desired fragments were confirmed by sequencing, they were sequentially moved into the pCDFDuet-1 bacterial expression plasmid which contained NcoI, AscI, SalI, and HindIII restriction sites in the desired sequence and orientation for building the full DNA constructs (Figure 4). Each of the unique A fragments and the pCDF backbone were isolated by double digestion with NcoI and AscI enzymes. The backbone and fragments were combined in a vector to insert ratio of 1:3 and ligated using T4 DNA ligase according to NEB protocol. Meanwhile, each of the unique C fragments and the pCDF2.1 vector containing the B fragment were isolated by sequential digestion with

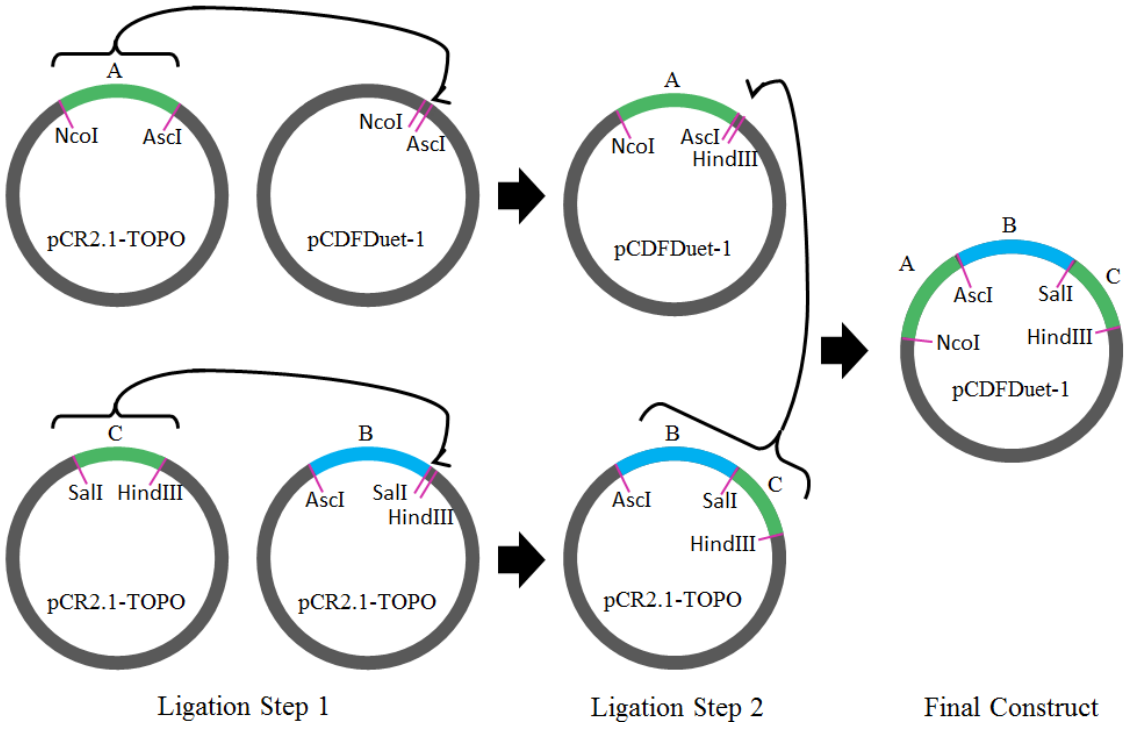

Figure 4 – Ligation method for creating final constructs. Two ligation steps combine fragments A, B and C into expression vector pCDFDuet-1. For C7, fragment B was added to pCR2.1-TOPO containing fragment C via digestion with SalI and EcoRV. The EcoRV site is just upstream of the cloning site in pCR2.1-TOPO.

SalI and HindIII enzymes and the C fragments were ligated adjacent to the B fragment. The plasmids containing adjacent BC fragments were then double digested with AscI and HindIII and ligated into the double digested pCDFDuet-1 vector containing the A fragment that corresponded to the C fragment insert. Wild type iRFP (WT iRFP) was also cloned from the pBAD/His-B vector into pCDFDuet-1 with NcoI and HindIII sites.

The only exception to this cloning protocol was for construct 7 which had a C fragment less than 100 bp in length. For this construct, fragment B was cloned into the pCR2.1 vector containing fragment 7C with cutting and ligating at sites NcoI and SalI. Then the BC adjacent fragment was ligated into the pCDFDuet-1 vector containing the fragment 7A. For each cloning step, digested plasmids were run on 0.7% agarose gels and the desired inserts and backbones were extracted from the gel using a QIAquick Gel Extraction kit. After each ligation reaction, the fresh ligation products were transformed into DH5α cells and plated overnight. Colonies were selected from the plates for 10 mL overnight cultures and plasmid isolation the next morning. Digestions were performed on the purified plasmids to determine which colonies contained the successful ligation product.

Protein Purification and Optical Characterization

Due to difficulties with obtaining A and C fragments for construct 4, only the full DNA constructs (C1, C2, C3, C5, C6 and C7) and the WT iRFP gene were transformed into BL21 PLysS competent cells along with the pAT-BV vector obtained from Clark Lagarias for coexpression of heme oxygenase (HO1), which provides biosynthesis of biliverdin from endogenous heme in E. coli for iRFP chromophore formation [34]. Colonies were selected with all of three antibiotics: 50 μg/mL spectinomycin (for

pCDFDuet-1 vector containing WT iRFP and constructs), 50 μg/mL kanamycin (for pAT-BV) and 34 μg/mL chloramphenicol (for the PLysS plasmid in the BL21 competent cells). Individual colonies were inoculated into 50 mL cultures in Luria-Bertani (LB) broth containing antibiotics and incubated at 37° C overnight. The next morning, the overnight cultures were diluted to an optical density (OD) of 0.1 at 600 nm into 1 L of LB medium containing 0.1 mM δ-aminolevulinic acid (ALA) and 0.05 mM $FeCl_3$ and incubated at 30° C until reaching 0.6 OD. The addition of ALA and $FeCl_3$ helps to facilitate production of heme for subsequent catabolism into biliverdin. At 0.6 OD, expression was induced with 1 mM Isopropyl β-D-1-thiogalactopyranoside (IPTG) except for a WT iRFP culture used as the noninduced control. Expression was continued at 30° C for 4 hours. Cells were then incubated on ice for 5 min, spun at 3,000 RPM for 20 min at 4° C, resuspended in 20 mL of 20 mM Tris pH 7.5 and spun again. Supernatants were discarded and cell pellets were frozen.

All frozen pellets were resuspended in 30 mLs lysis buffer (50 mM monobasic sodium phosphate (NaH_2PO_4) and 300 mM sodium chloride (NaCl)) and sonicated for 5 min on ice with 10 s cycle length and 50% duty cycle. Lysates were spun at 15,000 RCF for 45 min at 4° C. The supernatant was incubated with 250 μL of 50% HisLink Ni-NTA bead slurry from Promega overnight at 4° C in a rotorack to preferentially bind the His-tagged constructs and WT iRFP for purification. Ni-NTA beads were washed and eluted sequentially with 50 mM, 250 mM and 500 mM imidazole the next morning to obtain purified constructs and WT iRFP. The purified constructs and WT iRFP were then dialyzed into MOPS buffer with 15 kDa cutoff dialysis tubing to remove imidazole and stored at 4° C.

Absorbance spectra from 250 to 800 nm were obtained for the constructs and WT iRFP using a spectrophotometer. Excitation and emission spectra were also obtained from 550 to 800 nm with excitation at 700 nm and emission at 715 nm; 400 μL aliquots of the purified protein were spiked with either 40 mM EDTA to chelate any free Ca^{2+} or 20 mM $CaCl_2$. Absorbance and fluorescence spectra were also obtained for these aliquots to find any changes between the non-Ca^{2+} bound constructs and Ca^{2+}-bound constructs.

RESULTS

PCR yielded all required fragments for building constructs 1, 2, 3, 5, 6 and 7. Fragment sequencing revealed a silent mutation in fragment 1A at 260 bp and a removal of three nucleotides from 3A such that it contained only five His residues instead of six in the His tag, keeping the length of the fragment in frame. Multiple PCR attempts at fragment B amplification resulted in deleterious mutations. Two clones of fragment B containing mutations on opposite sides of a ClaI restriction site were cut with ClaI and XbaI to isolate the nonmutated regions of each clone. These regions were then ligated together to obtain a nonmutated version of fragment B, confirmed by sequencing.

None of the initial attempts at PCR amplification for fragments 4A or 4C were successful. After increasing the concentration of $MgCl_2$ to 3 mM to promote primer binding, some products of the right size were obtained but were also fraught with mutations. Construct 4 was therefore abandoned with attention turned to the other successfully generated construct fragments. 5A and 7A were able to be obtained using the newly designed primers and QIAGEN Multiplex PCR kit.

Initial attempts at ligation consisted of combining all digested fragments A, B and C with the cut pCDF backbone. However, ligation efficiency was too low to generate colonies after transformation due to the low probability of all four ligation sites coming together in the same reaction. Thus, the stepwise ligation procedure was preferred, though it was considerably more tedious and time-consuming. Ligations eventually

successfully generated each of the six remaining full constructs, confirmed by restriction enzyme double digestion with NcoI/AscI (for fragment A) and NcoI/HindIII (for full length) (Figure 5). Sequencing results with PACYCDuetUP1 and DuetDOWN-1 primers for the entire constructs also confirmed proper fragment arrangement.

Previous attempts at expression using 10 L fermenter auto-induction resulted in production of WT iRFP but not any of the novel constructs. We learned this by submitting the FPLC purified protein SDS PAGE gel band thought to be the novel constructs for mass spec. The mass spec results came back positive for E. coli lac repressor. The fermenter method may yet prove successful with culturing at 30° C and possibly require addition of IPTG. However, we turned to smaller-scale 1 L IPTG inductions with culturing in shaker flasks. IPTG-induced expression resulted in production of correct sized WT iRFP (~38 kDa) and remaining constructs (~55 kDa), confirmed by α-His probed western blot of the total lysates from each culture (Figure 6).

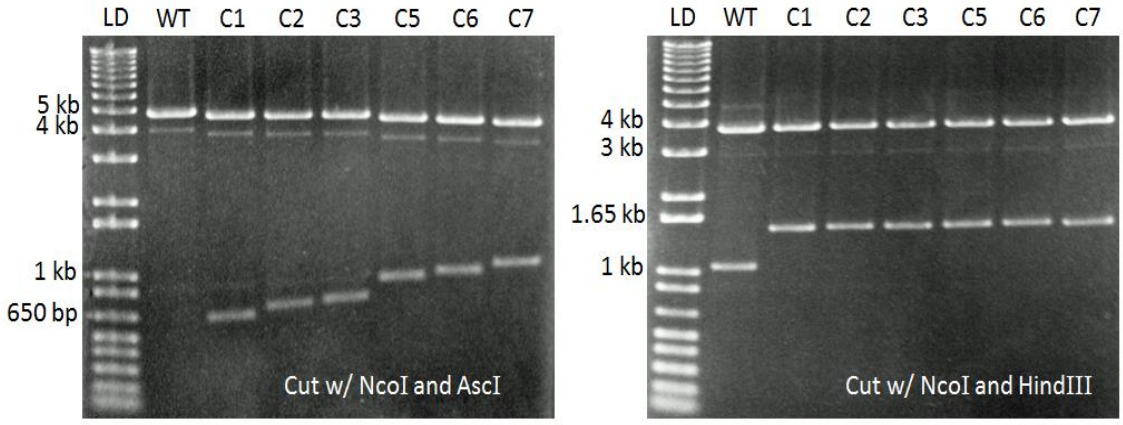

Figure 5 – Digestion confirming proper fragment construction. Lanes include DNA digestion of wild type iRFP (WT) and final constructs (C1-C7, excluding C4). Lower bands on left gel are fragment As. Lower bands on right gel are entire gene lengths. The 450 bp increase in molecular weight for the constructs from WT is due to CaM insert.

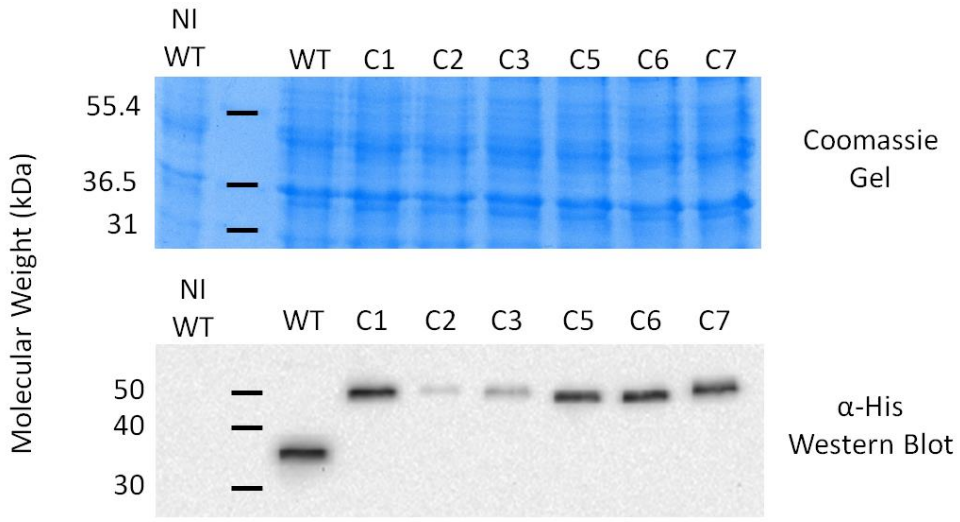

Figure 6 – Expression results for WT iRFP and constructs. Coomassie stained gel (top) and α-His stained western blot (bottom) of total lysates from noninduced culture (NI), wild type (WT) (38.6 kDa) and constructs (C1-C7, excluding C4) (55 kDa).

C2 and C3 showed significantly less expression than the other constructs, possibly due to less protein stability. During Ni-NTA purification, WT iRFP and C1 were a noticeably green color when bound to the beads and following elution. The noninduced control displayed no color and had no His-tagged proteins in the total lysate.

It is interesting to note that all of the bacteria cultures used for construct expression also co-expressed HO for biliverdin production. However, only expression of HO and WT iRFP or C1 together resulted in bacteria cells with green hue (Figure 7). Expression of HO alone resulted in normal colored cells. While we know that our expression method does result in degradation of endogenous heme for biliverdin production, it appears that expression of HO was not continued long enough to produce excessive amounts of biliverdin.

The absorbance spectrum for WT iRFP showed peaks at 280, 390 and 695 nm with a shoulder at 638 nm on the left side of the 695 nm peak as has been previously

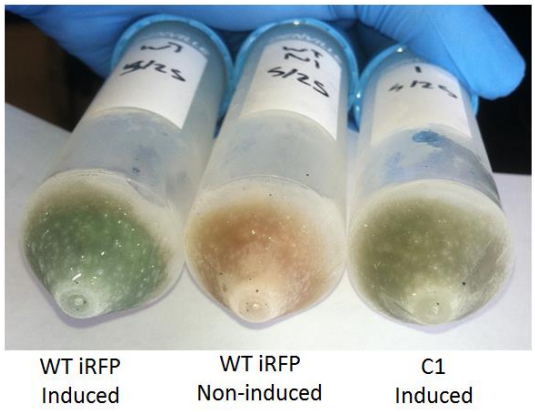

Figure 7 – Pelleted cultures showing green hue for WT iRFP and C1. The green color of WT iRFP and C1 are due to chromophore formation with biliverdin. Color of noninduced WT iRFP is that of normal E. coli.

reported [30]. When compared to the absorbance spectrum of free biliverdin with nearly the same peak height at 390 nm, obvious chromophore formation is visible in the WT iRFP sample compared to the very low peak in free biliverdin at 695 nm (Figure 8).

Excitation and emission spectra for WT iRFP had peaks at 695 and 713 nm, respectively. Our excitation and emission spectra show large peaks with 20 nm base widths appearing at 2 nm lower than the excitation wavelength in the emission spectra and at 2 nm higher than the emission wavelength monitored in the excitation spectra. These peaks suggest that the detector is picking up excitation wavelength light from the light source. These peaks may be eliminated by adjusting time delay between the source flash and photomultiplier integration of the emission signal or by narrowing slit width.

Batch purification of C1 successfully yielded elution fractions containing the construct (Figure 9). The absorbance spectrum for construct 1 had similar absorbance peaks to WT iRFP with the exception of a 5 nm peak shift and decrease in height from the WT iRFP 695 nm peak, placing C1's peak at 700 nm (Figure 10). Excitation and

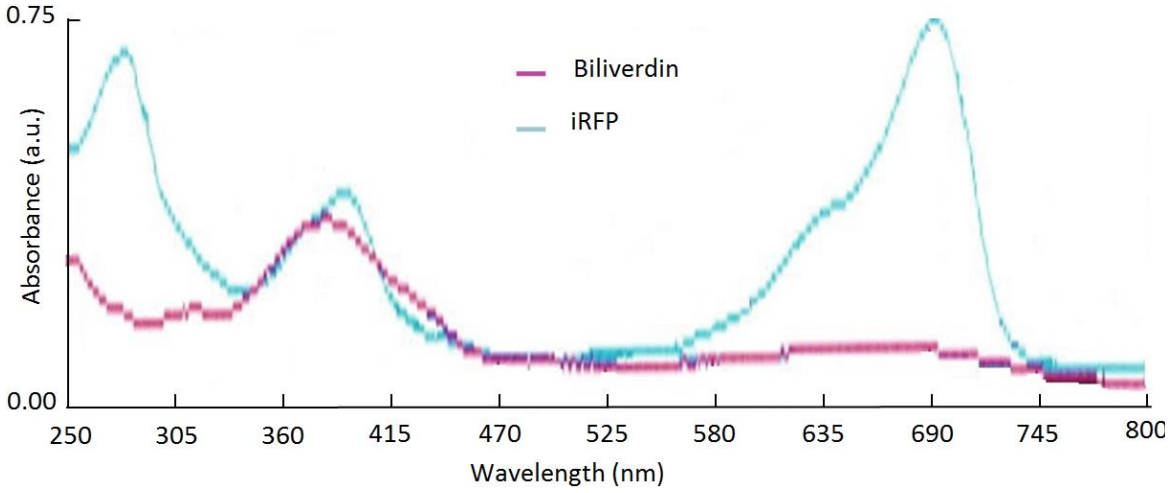

Figure 8 – Absorbance spectra for iRFP and free biliverdin. Incorporation of biliverdin into the chromophore binding pocket of iRFP results in an increase in the 695 nm peak with respect to the 390 nm peak.

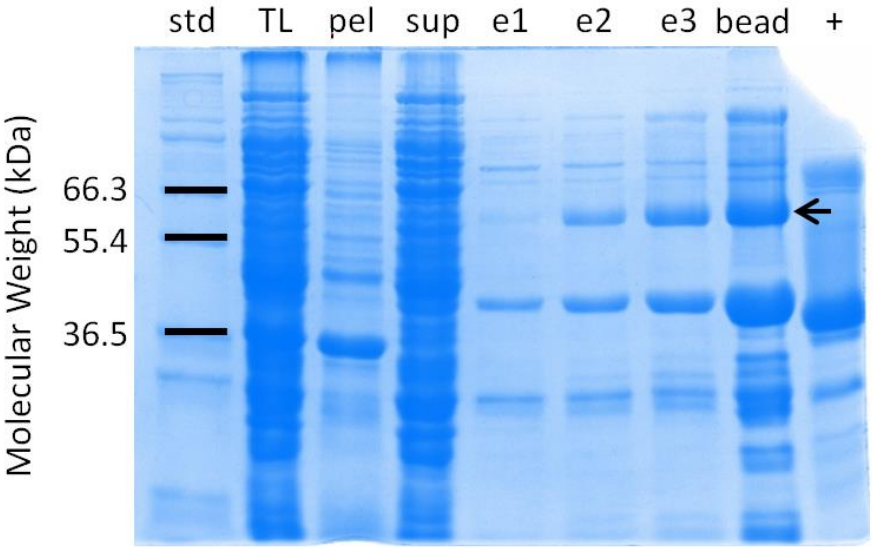

Figure 9 – Ni-NTA batch purification of C1. Arrow shows the eluted C1 protein at the expected 55 kDa molecular weight. std = standard, TL = total lysate, pel = pellet, sup = supernatant, e1 = elution in 50 mM imidazole, e2 = elution in 250 mM imidazole, e3 = elution in 500 mM imidazole, bead = Ni-NTA beads after elutions, + = positive control wild type iRFP for size comparison.

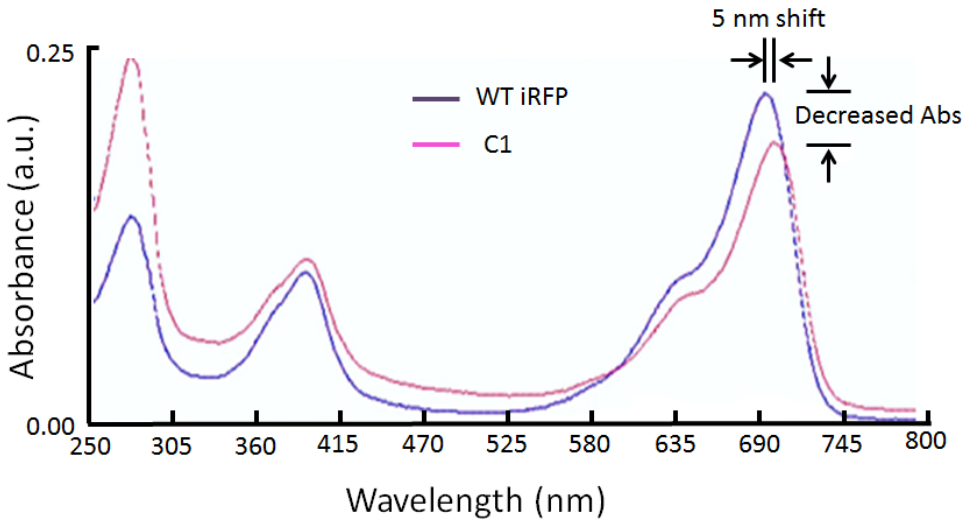

Figure 10 – Absorbance spectra for WT iRFP and C1. Note the wavelength shift from 695 nm for WT iRFP to 700 nm for C1 along with a decrease in maximum absorbance at the longer wavelengths with comparable 390 nm peak heights.

emission spectra for construct 1 were also similar to WT iRFP, though seemingly lower in amplitude. However, these traces were not normalized to total chromophore concentration as represented by the 390 nm absorbance peak so this difference in peak height could simply be due to lower amount of present chromophore.

Addition of 40 mM EDTA to aliquots of the purified WT iRFP and C1 or addition of 20 mM $CaCl_2$ had no effect on the absorbance spectra except for a high rise in absorbance at less than 280 nm for the EDTA samples. This had no interference with the biliverdin absorbance peak or the chromophore absorbance peak. Emission spectra were acquired for C1 without and with calcium saturation (Figure 11). No observable difference was seen between the EDTA and $CaCl_2$ conditions. However, due to the limited amount of purified protein, no duplicate or triplicate measurements could be taken for a statistical analysis. Therefore, these studies must be repeated upon purification of additional protein.

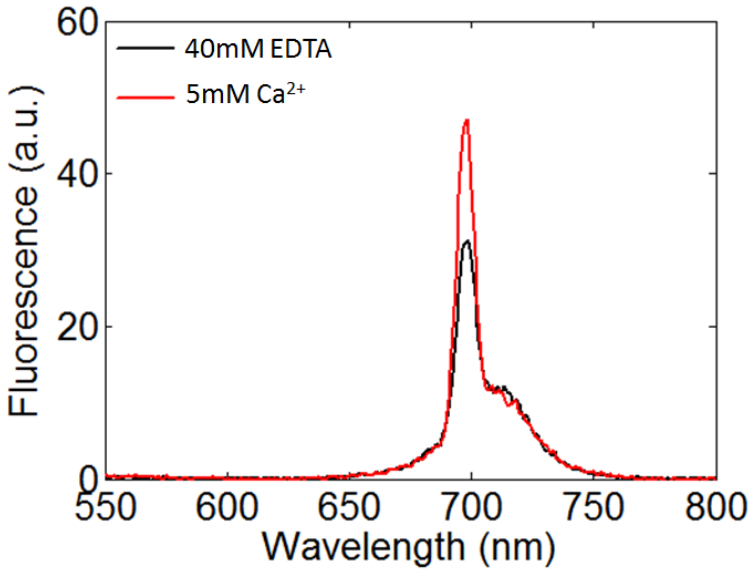

Figure 11 – Emission spectra for C1 in the absence and presence of calcium ions. Results are inconclusive for calcium sensitivity test on C1 emission. The large peak in each trace is thought to be artifact from the light source. Statistical analysis is not available due to N of 1 for the experiment.

DISCUSSION

Our results for expression of construct 1 show that receptor insertion into iRFP can be accomplished with successful binding of the biliverdin chromophore. This success holds exciting new possibilities for GECI engineering which has been limited to GFP variants up to this point. Though more conclusive studies with C1 fluorescence changes in the absence or saturation of Ca^{2+} may prove C1 to be Ca^{2+} insensitive, we have demonstrated the possibility that a different insert could lead to a successful infrared GECI.

Experimental determination of fluorescence sensitivity of calcium probes to Ca^{2+} is typically performed by measuring emission wavelength fluorescence intensity in aliquots of the purified protein containing various concentrations of Ca^{2+}, usually ranging from 10^{-10} to 10^{-2} M. If construct 1 is a feasible GECI, we should see a sigmoidal response from a minimal fluorescence intensity value at 10^{-10} M Ca^{2+} to a maximum fluorescence value at 10^{-2} M Ca^{2+}. Because we selected CaM as the insert, similar to camgaroo, we would also expect the sigmoidal curve to cross the 50% maximal fluorescence intensity level somewhere around 10^{-6} M. Excitation and emission spectra may also be obtained for each sample to check for any changes in peak wavelengths. If such shifts do occur, construct 1 may be ratiometric, allowing more quantitative measurement of Ca^{2+} concentration.

While our primary focus is in demonstrating successful receptor insertion into iRFP, CaM, with an overall K_d of around 10 μM, is a less than ideal insert for visualizing $[Ca^{2+}]_i$ fluctuations in cardiomyocyte or neuron cytosol which range from 100 nm to 1.3 μM [2]. With such a low Ca^{2+} affinity, very few of the infrared GECI containing the CaM insert would bind Ca^{2+} at peak $[Ca^{2+}]_i$, though CaM inserts resulting in affinities of greater than 2 μM have proven effective for monitoring $[Ca^{2+}]$ in the ER or mitochondria. The GECI engineering techniques that have resulted in K_d values ideal for cardiomyocyte cytosolic calcium transient imaging require the additional use of M13 in a circular permutation of the fluorescent protein or in conjunction with a second fluorescent protein with excitation wavelength near the emission wavelength of the first fluorescent protein to produce FRET between the two. The latter method may be accomplished with use of eqFP670, a red-shifted variant of katushka, a protein isolated from the E. quadricolor sea anemone [35]. eqFP670 exhibits emission at 670 nm which can excite iRFP, but may only result in half the excitation energy required for maximum emission intensity from iRFP. This scenario is likely more feasible than the circular permutation approach using CaM and M13 due to iRFP's different structure as compared to GFP.

Compared to GFP's structure of a ß barrel surrounding a residue-derived chromophore, iRFP is composed of a knot-like structure with two domains [31]. The PAS domain is the N terminal of iRFP and contains the Cys residue that covalently binds to biliverdin. The C terminal is contained by the GAF domain which comprises the chromophore binding pocket. The N terminal of the PAS domain is surrounded by a large loop of the GAF domain, forming the knot. Though GFP is known to self-assemble into its properly folded structure, iRFP is not known to behave this way, making successful receptor insertion of a 150 residue domain even more significant. However, iRFP's knot-

like structure and the large distance between the N and C terminals make circular permutation unlikely.

Other inserts have provided GECIs with higher Ca^{2+} binding affinity such as TN-humcTnC, which contains only sites I-III of TnC's EF hand motifs as the insert between cyan fluorescent protein (CFP) and citrine [21]. TN-humcTnC has a K_d of only 470 nM, which is similar to the affinity of the widely used rhod-2 calcium dye. This affinity is comparable to the C terminal domain of TnC. Similar inserts may be tried comprising other EF hand motifs from either CaM or TnC.

The crystal structure of C1 would be of benefit for analyzing possible mutations or insert modifications that would have greater possibility of affecting chromophore structure by conformational change of the insert upon chelation of Ca^{2+}. Molecular modeling may also be utilized once a solved structure is available for iRFP and C1, though such computational modeling of whole protein structural behavior is lengthy and computationally intensive. Once a successful insert is found with or without molecular modeling, the infrared GECI can also be subjected to site-directed mutations with high throughput FACS sorting to determine mutants with the most practical Ca^{2+}-binding affinities and fluorescence properties for use in the desired imaging application.

The applications for an infrared GECI will be diverse from improving current GECI studies by providing increased signal to noise ratio to novel noninvasive applications with possible pseudo-3D calcium mapping. Due to the noninvasive nature of an infrared GECI, longitudinal studies may also be performed on the same animal over the course of disease development or treatment with inducible infrared GECI expression at different stages of the disease or treatment [36]. Our understanding of changes in calcium handling will improve as we implement this novel noninvasive calcium probe.

REFERENCES

[1] D. Clapham, "Calcium signaling," *Cell*, pp. 1047–1058, 2007.

[2] H. J. Knot, I. Laher, E. A. Sobie, S. Guatimosim, L. Gomez-Viquez, H. Hartmann, L.-S. Song, W. J. Lederer, W. F. Graier, R. Malli, M. Frieden, and O. H. Petersen, "Twenty years of calcium imaging: cell physiology to dye for," *Molecular Interventions*, vol. 5, no. 2, pp. 112–27, Apr. 2005.

[3] S. M. Gagné, S. Tsuda, M. X. Li, L. B. Smillie, and B. D. Sykes, "Structures of the troponin C regulatory domains in the apo and calcium-saturated states," *Nature Structural Biology*, vol. 2, no. 9, pp. 784–9, Sep. 1995.

[4] G. P. C. Drummen, "Fluorescent probes and fluorescence (microscopy) techniques--illuminating biological and biomedical research," *Molecules (Basel, Switzerland)*, vol. 17, no. 12, pp. 14067–90, Jan. 2012.

[5] T. Knöpfel, J. Díez-García, and W. Akemann, "Optical probing of neuronal circuit dynamics: genetically encoded versus classical fluorescent sensors," *Trends in Neurosciences*, vol. 29, no. 3, pp. 160–6, Mar. 2006.

[6] A. P. de Silva, H. Q. N. Gunaratne, T. Gunnlaugsson, A. J. M. Huxley, C. P. McCoy, J. T. Rademacher, and T. E. Rice, "Signaling recognition events with fluorescent sensors and switches," *Chemical Reviews*, vol. 97, no. 5, pp. 1515–1566, Aug. 1997.

[7] G. Grynkiewicz, M. Poenie, and R. Y. Tsien, "A new generation of Ca^{2+} indicators with greatly improved fluorescence properties," *The Journal of Biological Chemistry*, vol. 260, no. 6, pp. 3440–50, Mar. 1985.

[8] K. R. Gee, K. A. Brown, W. N. Chen, J. Bishop-Stewart, D. Gray, and I. Johnson, "Chemical and physiological characterization of fluo-4 Ca^{2+}-indicator dyes," *Cell Calcium*, vol. 27, no. 2, pp. 97–106, Mar. 2000.

[9] G. Hajnoczky, L. D. Robb-Gaspers, M. B. Seitz, and A. P. Thomas, "Decoding of cytosolic calcium oscillations in the mitochondria," *Cell*, vol. 82, no. 3, pp. 415–424, Aug. 1995.

[10] M. Kamiya and K. Johnsson, “Localizable and highly sensitive calcium indicator based on a BODIPY fluorophore,” *Analytical Chemistry*, vol. 82, no. 15, pp. 6472–9, Aug. 2010.

[11] A. Matsui, K. Umezawa, Y. Shindo, T. Fujii, D. Citterio, K. Oka, and K. Suzuki, “A near-infrared fluorescent calcium probe: a new tool for intracellular multicolour Ca^{2+} imaging,” *Chemical Communications (Cambridge, England)*, vol. 47, no. 37, pp. 10407–9, Oct. 2011.

[12] P. Lee, F. Taghavi, P. Yan, P. Ewart, E. A. Ashley, L. M. Loew, P. Kohl, C. Bollensdorff, and C. E. Woods, “In situ optical mapping of voltage and calcium in the heart,” *PloS One*, vol. 7, no. 8, p. e42562, Jan. 2012.

[13] M. Brini, R. Marsault, C. Bastianutto, J. Alvarez, T. Pozzan, and R. Rizzuto, “Transfected aequorin in the measurement of cytosolic Ca^{2+} concentration,” *Journal of Biological Chemistry*, vol. 270, pp. 9896-903, Apr. 1995.

[14] J. E. McCombs and A. E. Palmer, “Measuring calcium dynamics in living cells with genetically encodable calcium indicators,” *Methods (San Diego, Calif.)*, vol. 46, no. 3, pp. 152–9, Nov. 2008.

[15] S. Direnberger, M. Mues, V. Micale, C. T. Wotjak, S. Dietzel, M. Schubert, A. Scharr, S. Hassan, C. Wahl-Schott, M. Biel, G. Krishnamoorthy, and O. Griesbeck, “Biocompatibility of a genetically encoded calcium indicator in a transgenic mouse model,” *Nature Communications*, vol. 3, p. 1031, Jan. 2012.

[16] O. J. Müller, B. Leuchs, S. T. Pleger, D. Grimm, W.-M. Franz, H. A. Katus, and J. A. Kleinschmidt, “Improved cardiac gene transfer by transcriptional and transductional targeting of adeno-associated viral vectors,” *Cardiovascular Research*, vol. 70, no. 1, pp. 70–8, Apr. 2006.

[17] T. Mao, D. H. O’Connor, V. Scheuss, J. Nakai, and K. Svoboda, “Characterization and subcellular targeting of GCaMP-type genetically-encoded calcium indicators,” *PloS One*, vol. 3, no. 3, p. e1796, Jan. 2008.

[18] G. S. Baird, D. A. Zacharias, and R. Y. Tsien, “Circular permutation and receptor insertion within green fluorescent proteins,” *Proceedings of the National Academy of Sciences*, vol. 96, no. 20, pp. 11241–11246, Sep. 1999.

[19] J. Nakai, M. Ohkura, and K. Imoto, “A high signal-to-noise Ca^{2+} probe composed of a single green fluorescent protein,” *Nature Biotechnology*, vol. 3, pp. 137–141, 2001.

[20] A. Miyawaki, J. Llopis, R. Heim, J. M. McCaffery, J. A. Adams, M. Ikura, and R. Y. Tsien, “Fluorescent indicators for Ca^{2+} based on green fluorescent proteins and calmodulin,” *Nature*, vol. 388, no. 6645, pp. 882–887, Aug. 1997.

[21] N. Heim and O. Griesbeck, “Genetically encoded indicators of cellular calcium dynamics based on troponin C and green fluorescent protein,” *The Journal of Biological Chemistry*, vol. 279, no. 14, pp. 14280–6, Apr. 2004.

[22] J. Akerboom, J. D. V. Rivera, M. M. R. Guilbe, E. C. A. Malavé, H. H. Hernandez, L. Tian, S. A. Hires, J. S. Marvin, L. L. Looger, and E. R. Schreiter, “Crystal structures of the GCaMP calcium sensor reveal the mechanism of fluorescence signal change and aid rational design,” *The Journal of Biological Chemistry*, vol. 284, no. 10, pp. 6455–64, Mar. 2009.

[23] S. Linse, A. Helmersson, and S. Forsén, “Calcium binding to calmodulin and its globular domains,” *The Journal of Biological Chemistry*, vol. 266, no. 13, pp. 8050–4, May 1991.

[24] T. Porumb, P. Yau, T. S. Harvey, and M. Ikura, “A calmodulin-target peptide hybrid molecule with unique calcium-binding properties,” *Protein Engineering*, vol. 7, no. 1, pp. 109–115, 1994.

[25] P. Mercier, M. X. Li, and B. D. Sykes, “Role of the structural domain of troponin C in muscle regulation: NMR Studies of Ca 2 + Binding and Subsequent Interactions with Regions 1-40 and 96-115 of Troponin I,” *Biochemistry*, vol. 39, pp. 2902–2911, 2000.

[26] E. W. Clemmens, M. Entezari, D. A. Martyn, and M. Regnier, “Different effects of cardiac versus skeletal muscle regulatory proteins on in vitro measures of actin filament speed and force,” *The Journal of Physiology*, vol. 566, no. Pt 3, pp. 737–46, Aug. 2005.

[27] M. X. Li, S. M. Gagné, S. Tsuda, C. M. Kay, L. B. Smillie, and B. D. Sykes, “Calcium binding to the regulatory N-domain of skeletal muscle troponin C occurs in a stepwise manner,” *Biochemistry*, vol. 34, no. 26, pp. 8330–40, Jul. 1995.

[28] V. Pansare, S. Hejazi, W. Faenza, and R. K. Prud’homme, “Review of long-wavelength optical and NIR imaging materials: contrast agents, fluorophores and multifunctional nano carriers,” *Chemistry of Materials: A Publication of the American Chemical Society*, vol. 24, no. 5, pp. 812–827, Mar. 2012.

[29] V. Ntziachristos, “Fluorescence molecular imaging,” *Annual Review of Biomedical Engineering*, vol. 8, pp. 1–33, Jan. 2006.

[30] G. S. Filonov, K. D. Piatkevich, L.-M. Ting, J. Zhang, K. Kim, and V. V. Verkhusha, “Bright and stable near-infrared fluorescent protein for in vivo imaging,” *Nature Biotechnology*, vol. 29, no. 8, pp. 757–61, Aug. 2011.

[31] X. Yang, E. A. Stojkovic, J. Kuk, and K. Moffat, “Crystal structure of the chromophore binding domain of an unusual bacteriophytochrome, RpBphP3, reveals residues that modulate photoconversion,” *Proceedings of the National Academy of Sciences of the United States of America*, vol. 104, no. 30, pp. 12571–6, Jul. 2007.

[32] R. Chattopadhyaya, W. E. Meador, A. R. Means, and F. A. Quiocho, “Calmodulin structure refined at 1.7 A resolution,” *Journal of Molecular Biology*, vol. 228, no. 4, pp. 1177–92, Dec. 1992.

[33] C. M. Johannessen, J. S. Boehm, S. Y. Kim, S. R. Thomas, L. Wardwell, L. A. Johnson, C. M. Emery, N. Stransky, A. P. Cogdill, J. Barretina, G. Caponigro, H. Hieronymus, R. R. Murray, K. Salehi-Ashtiani, D. E. Hill, M. Vidal, J. J. Zhao, X. Yang, O. Alkan, S. Kim, J. L. Harris, C. J. Wilson, V. E. Myer, P. M. Finan, D. E. Root, T. M. Roberts, T. Golub, K. T. Flaherty, R. Dummer, B. L. Weber, W. R. Sellers, R. Schlegel, J. A. Wargo, W. C. Hahn, and L. A. Garraway, “COT drives resistance to RAF inhibition through MAP kinase pathway reactivation,” *Nature*, vol. 468, no. 7326, pp. 968–72, Dec. 2010.

[34] G. A. Gambetta and J. C. Lagarias, “Genetic engineering of phytochrome biosynthesis in bacteria,” *Proceedings of the National Academy of Sciences of the United States of America*, vol. 98, no. 19, pp. 10566–71, Sep. 2001.

[35] D. Shcherbo, I. I. Shemiakina, A. V Ryabova, K. E. Luker, B. T. Schmidt, E. A. Souslova, T. V Gorodnicheva, L. Strukova, K. M. Shidlovskiy, O. V Britanova, A. G. Zaraisky, K. A. Lukyanov, V. B. Loschenov, G. D. Luker, and D. M. Chudakov, “Near-infrared fluorescent proteins,” *Nature Methods*, vol. 7, no. 10, pp. 827–9, Oct. 2010.

[36] M. T. Hasan, R. W. Friedrich, T. Euler, M. E. Larkum, G. Giese, M. Both, J. Duebel, J. Waters, H. Bujard, O. Griesbeck, R. Y. Tsien, T. Nagai, A. Miyawaki, and W. Denk, “Functional fluorescent Ca^{2+} indicator proteins in transgenic mice under TET control,” *PLoS Biology*, vol. 2, no. 6, p. e163, Jun. 2004.